Coastal Dynamics 2013
Paper No.

WAVE BOUNDARY LAYER DYNAMICS ON A LOW SLOPING LABORATORY BEACH

Dominic A. van der A[1], Dominique Mouazé[2], Laure Vignal[3], Paulo A. Silva[4], Tiago Abreu[5], Eric Barthélemy[3] and Hervé Michallet[3]

Abstract

Wave-induced cross-shore sediment transport is driven by non-linear processes such as boundary layer streaming, skewness and asymmetry, and the generation of infragravity waves. Most of our understanding of wave nonlinearity and associated wave boundary layer dynamics originates from studies involving relatively steep beach slopes (>1:40). Non-linearity on lower sloping beaches is expected to be of different character, which has prompted a series of laboratory experiments as part of the GLOBEX project on a 1:80 beach slope involving random, bichromatic and regular wave conditions. In this paper preliminary results are presented of high resolution wave boundary layer measurements in the surf zone obtained with a 2-component LDA system. The focus is on the time-averaged velocity near the bed, and the development of skewness and asymmetry within the boundary layer. Results show that for all conditions there is a strong decrease in velocity asymmetry within the boundary layer which coincides with an increase in velocity skewness, consistent with previous findings. When the vertical coordinate is appropriately scaled, a linear relationship appears between the velocity skewness in the boundary layer and the velocity asymmetry and skewness in the free-stream. Parameterizing this relationship for rough turbulent flow conditions could improve predictive capability of cross-shore sediment transport formulae.

Key words: Boundary layer flow, streaming, skewness, asymmetry, bichromatic waves

1. Introduction

Morphological development in the nearshore zone is a result of the complex interaction between the hydrodynamics, the sediments and the seabed itself. In the cross-shore direction, where the hydrodynamics are largely dominated by wave motion, sediment is transported primarily close to the sea-bed within the wave-induced oscillatory bottom boundary layer. Here, net (wave-averaged) sediment transport occurs as a direct result of wave-nonlinearity (e.g., Ribberink and Al-Salem, 1994; O'Donoghue and Wright, 2004; Ruessink et al., 2011; Van der A et al., 2010) or as a result of non-linear wave processes such as wave boundary layer streaming (Longuet-Higgins, 1953; Kranenburg et al., 2013) and the generation of infragravity waves. Infragravity waves are oscillatory motions in the sea surface with periods of 20 to 200s, and are particularly important close to the shore where they affect beach and dune erosion processes (e.g. Van Thiel de Vries et al., 2009). Detailed knowledge of the wave-induced boundary layer dynamics is therefore essential to understand cross-shore sediment transport processes and is key to the development of practical sediment transport formulae implemented in large-scale morphological models.

Non-linear waves exhibit skewness, i.e. high wave crests of short duration and shallow troughs of long duration, asymmetry, i.e. steep fronted sawtooth-shaped waves, or a combination of both. The degree of skewness and/or asymmetry depends on the proximity of the wave to the shoreline (Ruessink et al., 2012). Wave skewness and asymmetry, which are mirrored in the wave-induced oscillatory flow, remain constant throughout most of the water column. However, within the wave boundary layer, skewness and asymmetry alter rapidly. This variation results in a near bed flow and, thus a bed shear stress with a periodic behaviour

[1]School of Engineering, University of Aberdeen, Aberdeen AB24 3UE, Scotland. d.a.vandera@abdn.ac.uk
[2]M2C, UMR 6143, 24 rue des Tilleuls, 14000 CAEN, France, dominique.mouaze@unicaen.fr
[3]LEGI, CNRS, Université de Grenoble, BP53, F-38041 Grenoble CEDEX, France. laure.vignal@legi.grenoble-inp.fr, eric.barthelemy@legi.grenoble-inp.fr, herve.michallet@legi.grenoble-inp.fr
[4]CESAM & Department of Physics, University of Aveiro, 3810-193 Aveiro Portugal. psilva@ua.pt
[5]CESAM & Dep. of Civil Eng., Polytechnic Institute of Viseu, 3504-510 Viseu, Portugal. tabreu@estv.ipv.pt

that differs largely from the free-stream oscillatory flow. Hendersen et al. (2004) showed theoretically how free-stream asymmetry turns into near bed skewness as a result of the frequency-independent phase shift of the Fourier components, which results into a frequency dependant shift in the time domain of the different components of the velocity. Recently, Berni et al.'s (2013) mobile bed boundary layer measurements confirmed that free-stream asymmetry transforms within the boundary layer into skewness of the near-bed flow. Following the theoretical work of Henderson et al. (2004), they presented a method to describe the near-bed skewness in terms of the free-stream asymmetry and skewness. However, due to experimental limitations Berni et al. were only able to obtain reliable velocity measurements in the upper part of the wave-induced boundary layer. Consequently, it remains poorly understood how wave non-linearity is conveyed down the wave boundary layer. Non-linear boundary layer streaming is an additional process that can affect net sediment transport (e.g Kranenburg et al., 2013). Such streaming is found to be amplified under irregular wave groups (Yu et al., 2010) compared to the more studied regular wave conditions.

Wave non-linearity is paramount on both steep and low-sloping beaches, but is of different character. On steep beaches very strong non-linear processes happen locally and on a short time scale (as demonstrated by narrow surf zones with plunging or collapsing breakers), whereas the non-linearity on low-sloping beaches is significant because it builds up over a lengthy time over an extensive cross-shore area. Since most of our comprehension and predictive ability of nearshore processes have resulted from theoretical work, laboratory experiments, and field studies on beaches with slopes steeper than about 1:40, the case of strong non-linearity on low sloping beaches is not well documented; this knowledge gap led to the GLOBEX project (see Ruessink et al., 2013 for a project overview).

Due to the practical difficulties involved with obtaining detailed boundary layer measurements under full-scale waves in the field, much of our current understanding of wave-induced boundary layer flow originates from laboratory wave flume studies (Sleath, 1970; Klopman, 1994; Dixen et al, 2008) and oscillatory flow tunnel experiments (Jonsson and Carlsen, 1974; Sleath, 1987; Jensen et al., 1989; Van der A et al., 2011). Flow tunnels allow the oscillatory boundary layer to be studied at full-scale (in terms of Re and a/k_s), but the absence of the free surface and vertical velocity component lead to notable differences compared to the progressive wave induced boundary layer. In particular, oscillatory flow tunnels do not generate non-linear wave boundary layer streaming (Longuet-Higgins type) and degrees of non-linearity that can be generated are low and hence not representative of real waves in and around the breaker zone. Experimental study of these hydrodynamic conditions is more suited to wave flume facilities.

This paper reports on preliminary results obtained from a long wave flume as part of the Hydralab IV funded GLOBEX project. The particular focus is on non-linear boundary layer streaming and the vertical structure of velocity skewness and asymmetry. A better understanding of how velocity and acceleration skewness are conveyed down to water column is essential to accurate predictions bed shear stress and sediment transport. Another purpose of the boundary layer measurements was to obtain an estimate of the hydraulic roughness of the fixed experimental bed, which is an essential input to some of the numerical models applied within the project.

2. Experiments

2.1. *Experimental facility*

The experiments were conducted in the Scheldt Wave Flume at Deltares, the Netherlands. The flume is 110 m long, 1.0m wide and 1.2m high. Glass sidewalls are fitted along the flume, except in the central 10m of the flume length where the sidewalls are made of concrete. The piston type wave maker, equipped with Active Reflection Compensation (ARC), has a 2m stroke and is able to generate waves with a maximum wave height of H = 0.4m for regular waves and a maximum significant wave height of H_s = 0.25m for irregular waves. For the present experiments a 1:80 sloping impermeable concrete beach was constructed starting at x = 16.6m from the wave maker central position (which is the x = 0m datum). The still water depth at the wave maker was 0.85m for all experiments.

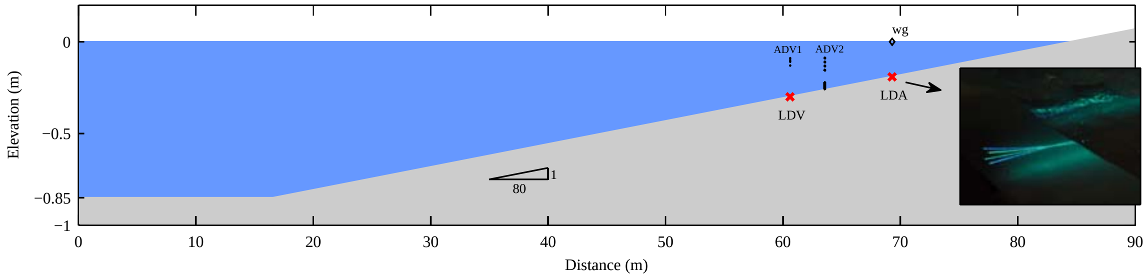

Figure 1. Cross-shore section of the Scheldegoot at Deltares illustrating the locations of the boundary layer measurements along the 1:80 beach profile. The photograph shows the two laser-beam pairs of the LDA system.

2.2. *Measurements*

Water surface elevation was measured using 22 wave gauges, 18 of which were mounted on moveable trolleys. Moving the trolleys between different runs allowed water surface measurements with very high spatial resolution, every 0.55m on the horizontal section and in the first part of the slope and at every 0.37m on the remainder of the slope, which covered the surf and swash zones. In this paper the results from the water surface measurements are used qualitatively to reference the boundary layer measurements to their measurement location in the nearshore zone. More detailed results from the wave gauge measurements are presented in Ruessink et al. (2013) and other GLOBEX reports mentioned therein.

Horizontal and vertical velocities in the wave boundary layer were measured at two different locations along the low sloping beach profile, using different instruments. At x = 60.6m a Deltares Laser Doppler Velocimeter (LDV) system was positioned together with an Acoustic Doppler Velocimeter (ADV) to obtain the free-stream velocity, while at x = 69.3m a Dantec Laser Doppler Anemometry system was located, hereafter referred to as the LDA system, see Figure 1. In addition to the boundary layer measurements, a side-looking ADV was positioned between the LDA system and the Deltares LDV system (x = 63.6m, y = 0.35m) to obtain a measure of the velocity profile in the water column above the wave boundary layer (z_{min} ≈ 6mm). In this paper we will report only on the measurements obtained with the LDA system.

2.1.1. *LDA measurements*

The 2D LDA system is a fibre optic system operating in back-scatter mode. The core system components are a 300mW Ar-Ion air-cooled laser, a 112mm fibre optic transducer probe, and a Dantec BSA F60 burst spectrum signal processor. The main laser beam was colour-separated into a green and blue line, each colour was split into pairs of equal intensity, of which one line was frequency shifted by 40Mhz using a Bragg Cell. The transducer probe has an internal beam expander and for the present experiment was fitted with a 500mm focal length lens, resulting in a measurement volume (ellipsoid) of 76μm diameter and 1.36mm length (in water). Because the probe is positioned somewhat in front of the glass sidewall the measurement location in y-direction was approximately y = -0.17m (where y = 0m is the flume centreline). In order to allow velocity measurements very close to the bed, the probe was rotated so that the two velocity components at 45° from the bed normal direction were measured. The horizontal and vertical velocity components were obtained by simple orthogonal transformation of these measured components. The probe was positioned by a computer-controlled 3D traversing system allowing the measurement volume to be positioned with an accuracy of 0.1mm. The local bed level (z = 0mm) was determined by gradually traversing the measurement volume towards the bed until the level where the periodic velocity signal had first disappeared and coincided with large photo-multiplier anode currents indicative of strong wall reflections. For test series A and B measurements were done at 18 elevations logarithmically spaced between z = 0.1mm and 10mm, while for series C the measurements extended to 50mm above the bed, consisting of 12 (C1) and 30 elevations (C2). Silver-coated hollow glass spheres with a diameter of 10μm were used to seed the flow, except during the first few days of testing when seeding material was unavailable. The lack of seeding resulted in poor data quality during the first two measurement elevations for series A and B, which were therefore omitted from further analysis. The still water depth at the LDA measurement location was 0.19m for all conditions and local wave set-up was of the order of a few mm's for each condition.

Because the LDA system only records a velocity when a seeding particle passes through the measurement volume the velocities are recorded irregularly. Phase-averaged (i.e. ensemble-averaged) u- and w-velocities for series B and C (see Table 1) were obtained by dividing each group/wave cycle of the time-series into equal length phase-intervals (equivalent to 1/32s) and applying so-called residence time weighting. The LDA system simultaneously recorded the local water surface elevation from a capacitance wave gauge positioned on the opposite side of the flume (y = 0.4m). By using the water surface measurement as a reference, the correct phase information of the velocity measurement at each z-level could be obtained. Phase-averaging was generally done over 90-140 group cycles for the Series B conditions and over 69 and 228 wave cycles for conditions C1 and C2, respectively.

2.3. *Test conditions*

The experimental programme comprised three test series (see Table 1). Series A involved JONSWAP random wave conditions with increasing wave height and period (A1 and A2), representing storm conditions, and condition A3 had a peak enhancement factor of γ = 20, representing energetic swell conditions. Series B involved bichromatic conditions, leading to a single infragravity wave with period T_g (i.e. "group" period). The difference between B2 and B3 lies in the amplitudes of the carrier waves, resulting in different amplitudes of the incoming infragravity wave. Series C involved one monochromatic infragravity condition with period equal to the group period of conditions B2 and B3. Condition C2 involved a monochromatic short wave condition, and was initially run to obtain a high resolution velocity profile close to the bed. The maximum wave dissipation (break point) was reached at about x = 60m for A2, Series B and C2, 70m for A1 and A3, and close to shore line (~80m) for C1.

Table 1. Test conditions.

Test Series A								
Condition	H_s (m)	T_p (s)			Re	a/k_s	δ (mm)	Remark
A1	0.10	1.6			$0.8 \cdot 10^4$	68	0.8	JONSWAP; γ = 3.3
A2	0.20	2.25			$1.5 \cdot 10^4$	92	0.9	JONSWAP; γ = 3.3
A3	0.10	2.25			$1.1 \cdot 10^4$	79	0.9	JONSWAP; γ = 20
Test Series B								
Condition	a_1 (m)	a_2 (m)	f_1 (Hz)	f_2 (Hz)	Re	a/k_s	δ (mm)	Remark
B1	0.09	0.01	6/15	7/15	$1.0 \cdot 10^4$	92	0.9	T_g = 15s; f_m = 0.43Hz
B2	0.09	0.01	0.42	0.462	$1.1 \cdot 10^4$	96	0.9	T_g = 23.8s; f_m = 0.44Hz
B3	0.07	0.03	0.42	0.462	$1.5 \cdot 10^4$	111	0.9	T_g = 23.8s; f_m = 0.44Hz
Test Series C								
Condition	H (m)	T (s)			Re	a/k_s	δ (mm)	Remark
C1	0.02	23.8			$7.0 \cdot 10^4$	778	2.9	$Re_h = 2.4 \cdot 10^4$
C2	0.20	2.25			$1.2 \cdot 10^4$	99	0.9	

Reynolds number Re is defined as $Re = \sqrt{2}u_{rms}a/\nu$, where kinematic viscosity $\nu = 1.19 \cdot 10^{-6}$ m^2/s is based on the average measured water temperature during the experiment, and orbital amplitude $a = \sqrt{2}u_{rms}/\omega$, with $\omega = 2\pi/T$. For test series A, ω was based on peak period, T_p, and for series B on the mean period, T_m. For all conditions u_{rms} was evaluated in the free-stream at z = 10mm above the bed, except for C1 where it was evaluated at z = 30mm. The ratio a/k_s is the relative roughness, where the Nikuradse roughness is estimated as $k_s \approx 0.7$mm (see Section 3.3), $\delta = (2\nu/\omega)^{0.5}$ is the (viscous) Stokes length. Figure 2 shows the present experiments amongst previous fixed bed studies (both from tunnel and wave flumes) in a Re-a/k_s diagram, indicating that the present conditions are all in the transitional regime between laminar and turbulent flow. Condition C1 represents a long shallow water wave with a near-bed orbital amplitude of a = 0.54m, which is an order of magnitude larger compared to the other conditions. Since a is much larger than the local water depth (h = 0.19m) it could be argued that h should be seen as the characteristic length scale. This result in a Reynolds number related to the water depth of $Re_h = 2.4 \cdot 10^4$, which would mean C1 is still in the transitional regime.

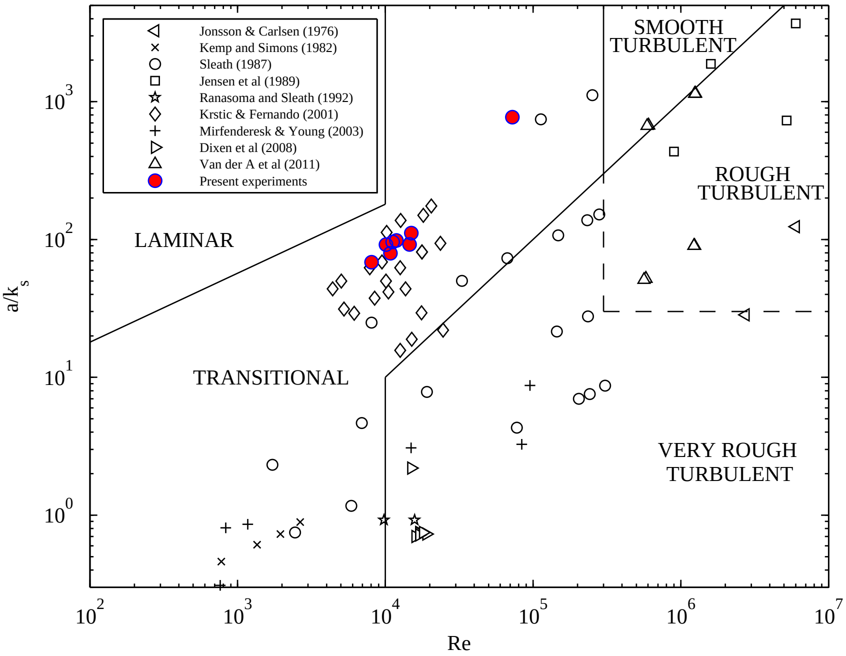

Figure 2. Delineation of flow regimes showing the present experiments amongst previous fixed bed studies (adapted from Van der A et al., 2011, references listed therein).

3. Results

3.1 *Phase-averaged velocities*

Figure 3 shows the phase-averaged velocity time-series at two elevations for the bichromatic condition B3 (T_g = 23.8s). The maximum boundary layer thickness (defined as the level of maximum overshoot) of the short waves is about 2-3mm. Therefore, the time-series at z = 10mm is in the free-stream, while the time-series at z = 0.5mm is located well into the boundary layer. In this figure only the oscillatory part of the velocity is shown, i.e. $\tilde{u} = \langle u \rangle - u_m$, where $\langle u \rangle$ is the phase-averaged velocity and u_m is the time-averaged velocity. Comparison of the velocities at both levels shows that at z = 0.5mm the velocity maxima have strongly decayed, and that the velocity at 0.5mm leads the free-stream velocity in phase, a well-known feature of wave-induced oscillatory flows.

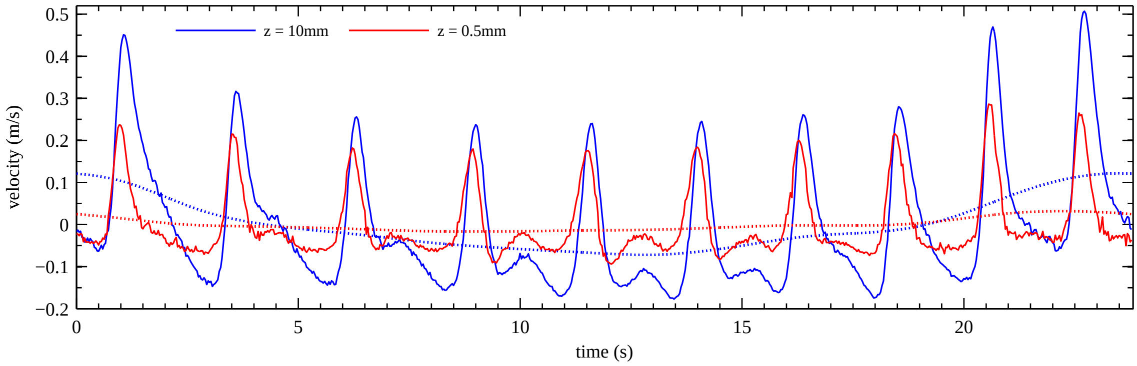

Figure 3. Example time-series of the ensemble-averaged oscillatory velocity $\tilde{u}$ in the free-stream (z = 10mm) and within the wave boundary layer (z = 0.5mm). The dashed lines indicate the low frequency velocity component, $\tilde{u}_{lf}$, obtained by low-pass filtering $\tilde{u}$. Condition B3.

The dashed lines represent the low-frequency part of the oscillatory velocity $\tilde{u}_{lf}$ which is obtained by low-pass filtering $\tilde{u}$ with a cut-off frequency of $0.5f_m$ Hz. This low-frequency orbital velocity is induced by the infra-gravity wave that is bound to the wave group. In the free-stream $\tilde{u}_{lf}$ displays a large onshore velocity which is of shorter duration compared to the much lower offshore velocity. This behaviour is indicative of a shoaling wave. The maximum infra-gravity velocity in the free-stream is 0.12m/s which is substantial compared to the maximum velocity of around 0.4m/s reached under the short waves alone at this elevation. At z = 0.5mm the infra-gravity velocity also leads the free-stream velocity but the maximum $\tilde{u}_{lf}$ has reduced to 0.03m/s, which is relatively much stronger reduction in velocity compared the short wave equivalent. The latter can be explained by the fact that the infra-gravity velocity component will have a much thicker boundary layer compared the short wave boundary layer, since the boundary layer thickness is proportional to $\sqrt{T}$, hence the velocity gradient near the bed is much smaller for the infra-gravity component.

Figure 4 shows the velocities for the long wave condition (condition C1). The wave period of this condition was equal to the infragravity wave period of condition B3. The velocity time-series shown in Figure 4a displays a distinct sawtooth-shape (asymmetric), with the maximum positive velocity being almost equal in magnitude to the maximum negative velocity. Figure 4b shows velocity profiles throughout the wave cycle, and demonstrates the distinct velocity overshoot near the bed. The boundary layer thickness at maximum positive flow is smaller compared to that at maximum negative flow. This is a result of the sawtooth shaped velocity time-series, where the boundary layer has less time to grow before maximum positive free-stream velocity is reached but comparatively longer time available until maximum negative free-stream velocity is reached. This leads to a larger velocity gradient and bed shear stress in the onshore direction, compared to the offshore direction, which in case of mobile beds and short waves will promote onshore sediment transport (van der A et al., 2010). However, because of the large boundary layer thickness and consequently small velocity gradients, the direct influence of the infragravity-wave on the mobilization of sediment is expected to be small compared to the short wave influence. Once sand has been brought into suspension to levels above the short wave boundary layer, the relatively large low-frequency velocities have the potential to impact the net sediment transport. This is especially true for finer sand associated with low-sloping beaches.

The mean velocity profile is shown in Figure 4c, it shows the positive onshore streaming near the bed, while for z > 10mm the mean flow is negative as result of the mass transport compensating return flow. Offshore-directed boundary layer streaming as a result of turbulence asymmetry between the onshore and offshore phase of the flow, is not expected to have contributed very much since C1 and the other conditions were are all in the transitional flow regime, close to laminar flow.

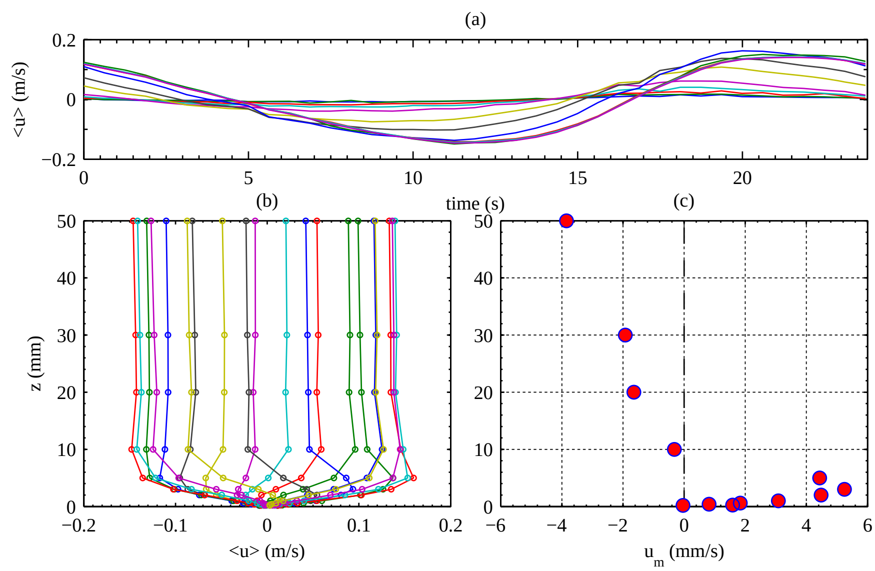

Figure 4. (a): time-series of ensemble-averaged velocity at selected elevations (z_{min} = 0.2mm; z_{max} = 50mm); (b): ensemble-averaged velocity profiles at 1.25s intervals; (c): time-averaged (mean) velocity profile. Condition C1.

3.2 *Streaming*

Figure 5 shows time-averaged velocities for all experimental conditions. For the random wave conditions (series A) there is near bed onshore streaming and negative return flow at high elevations. For conditions A1 and A3 the LDA measurement location was located in the outer surfzone. But for condition A2 it was located in the inner, well-developed surfzone (higher wave height) leading to a stronger undertow and consequently a reduction of the onshore streaming, which is limited to approximately z < 1mm. Condition A3 is similar in wave height and period to A1, but the spectral shape is more narrow banded (γ = 20, compared to γ = 3). The change from positive to negative mean flow occurs at a lower z which are caused by the stronger return flow as a result of more localized and intense wave-breaking.

For the bichromatic conditions, B1 and B2, and regular wave condition C2, there is also near-bed onshore streaming but there is no distinct negative mean velocity at higher elevations. Since the measurements only capture the bottom 10mm of the 190mm water column it is expected that mean velocity will change sign at z > 10mm. While measurements from EMF transducers mounted on the mobile trolley confirm this expectation for B1 and B2 (for C2 no corresponding EMF measurements were made) another explanation for this behaviour could be the presence of cross-modes in the wave flume. These were visually perceived especially for conditions B1 and B2 (and C2). Cross-modes will generate secondary motions which will have a height-dependant velocity component in the y-direction that may lead to non-zero vertical mean velocities. Figure 5 also includes the vertical mean velocities (crosses), which show that the vertical velocities at the upper elevations (> 2mm) are indeed non-zero for conditions B1, B2, and C2 and relatively large compared to the horizontal mean velocities. Preliminary results from ADV2 located at x = 63.6.m confirm the presence of substantial (mean) velocities in y-direction for these conditions. Additionally, images from ceiling-mounted video cameras that recorded the water surface elevation could give more detail on the structure of the cross-modes in the flume for these conditions, but this data has not been processed yet. However, since the mean flow is very small compared to the main oscillatory flow in x-direction the possible cross-mode effect on the instantaneous u velocities are generally expected to be small.

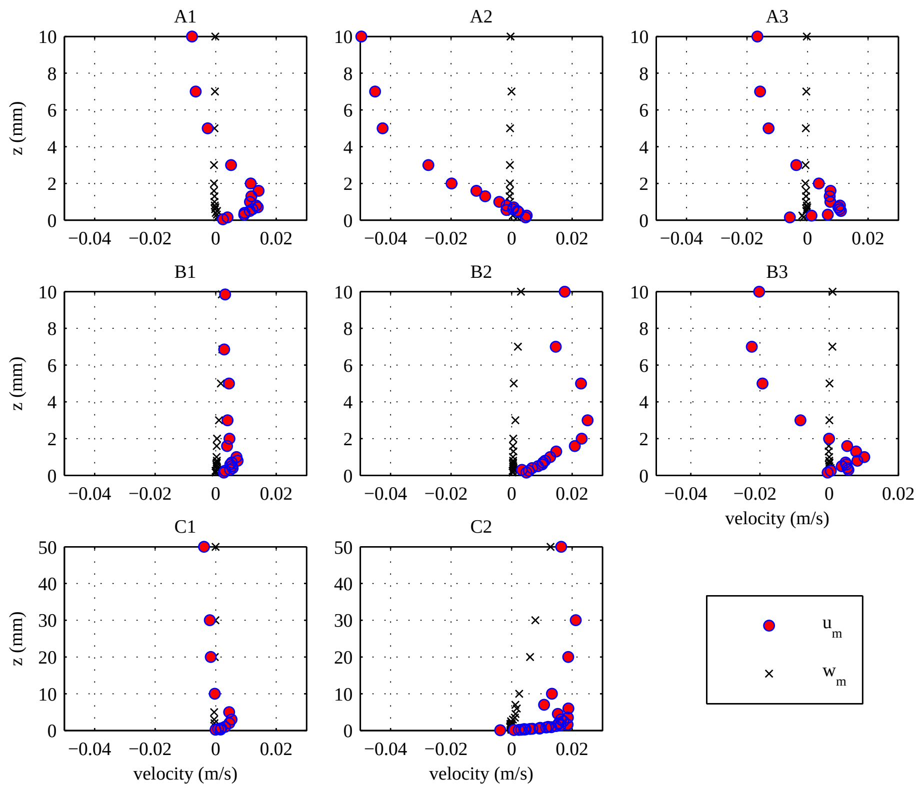

Figure 5. Time-averaged velocity profiles.

3.3 *Bed roughness*

To obtain an estimate of the bed roughness k_s the so-called velocity defect law (see Nielsen, 1992; Nielsen and Guard, 2010) is applied to the measured velocity profiles of the regular wave conditions C1 and C2. For a simple harmonic oscillatory flow the velocity in the boundary layer can be described by the complex defect function $D_1(z)$ as follows

$$u(z,t) = a\omega\left[1 - D_1(z)\right]e^{i\omega t} = a\omega\left[1 - \exp\left(-[1+i]\left(\frac{z}{z_1}\right)^p\right)\right]e^{i\omega t} \quad (1)$$

which for p = 1 and $z_1 = \delta = (2\nu/\omega)^{0.5}$ results in the smooth laminar boundary layer solution. Nielsen and Guard (2010) showed that an analysis of the primary harmonic of the velocity records enables a good description of the structure of oscillatory flow for different hydraulic regimes, when the vertical length scale z_1 is taken as a combination of the viscous length scale and rough length scale as follows

$$z_1 = \sqrt{0.008 k_s a + \delta^2} \quad (2)$$

From Eq. (1) it follows that $-ln|D_1| = 1$ at elevation $z = z_1$. Since $D_1(z)$ can be directly obtained from the measured velocities, the value of z_1 (and p) can be obtained by plotting $-ln|D_1|$ as a function of the elevation z (a more detailed description of the procedure is contained in Abreu et al., 2012), which is done in Figure 6 for conditions C1 and C2. For condition C1 we obtain z_1 = 3.5mm, which according to Eq. (2) corresponds to $k_s \approx$ 0.7mm. However, for condition C2 the length scale $z_1 \approx \delta$, implying (smooth) laminar flow. The reason for this discrepancy is not entirely clear. However, while at this stage no detailed attempts have been made to optimize the fits in Figure 6, it should be noted that applying a small offset of 0.1mm to the vertical coordinate of C2 (i.e. of the order of the accuracy of the traverse system and also approximately the vertical extent of the measurement volume), would result in $k_s \approx$ 0.35mm for that condition. Applying the same offset to vertical coordinate of condition C1 would only lead to ±0.2mm difference in k_s. In Figure 2 we have therefore adopted k_s = 0.7mm, whereby it is worth noting that using any of the k_s values reported before would not alter the classification of transitional flow for the present conditions.

Ongoing work is focussed at getting separate estimates of k_s by applying the log-law to the measured velocity profiles for the various conditions, and to obtain estimates of the bed shear stress.

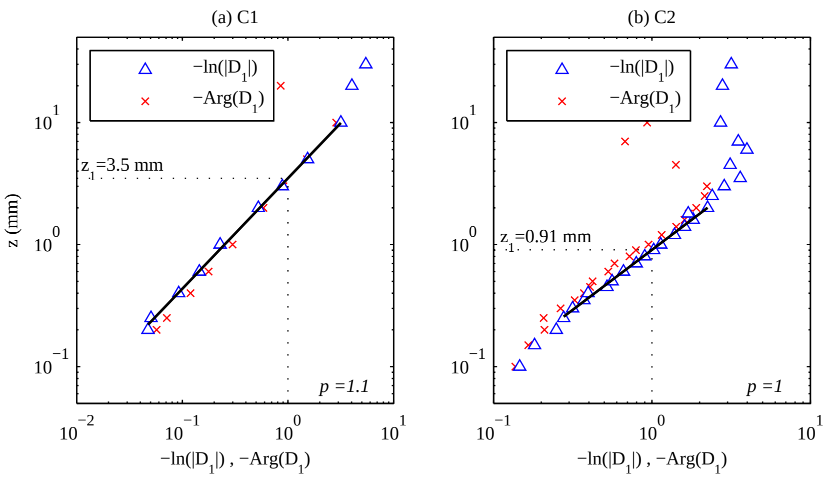

Figure 6. Vertical profiles of $-ln(|D_1|)$ and $-Arg(D_1)$ obtained from the velocity measurements for regular wave conditions C1 and C2. The black solid line represent the best linear fit through the straight part of $-ln(|D_1|)$ (on log-log scale), with p^{-1} the slope of the line. See Nielsen (1992) or Nielsen and Guard (2010) for an interpretation of $-Arg(D_1)$.

3.4 *Skewness and Asymmetry*

Orbital velocities induced by non-linear waves are characterized by their degree of skewness and asymmetry. Skewness (velocity skewness) is a relative measure of larger orbital velocities under the wave crest compared to the smaller velocities under the wave trough. Asymmetry (acceleration skewness) is the relative measure of larger accelerations between trough and crest compared to smaller accelerations between crest and trough (Malarkey and Davies, 2013). The dimensionless degrees of skewness and asymmetry at level *z* can be defined as

$$Sk(z) = \frac{\overline{\left(u(z,t) - \bar{u}(z)\right)^3}}{u_{\mathrm{rms}}^3(z)} \tag{3}$$

$$Asy(z) = -\frac{\overline{\mathrm{Im}\left(H\left(u(z,t)\right)\right)^3}}{u_{\mathrm{rms}}^3(z)} \tag{4}$$

with $H(u(z,t))$ the Hilbert transform of $u(z,t)$, *Im* the imaginary part, and overbar denotes time-averaging. For a sinusoidal wave $Sk = 0$ and $Asy = 0$. $Sk > 0$ indicates larger velocities in the onshore (crest) direction compared to the offshore (trough) direction, similarly $Asy > 0$ indicates larger accelerations in onshore direction.

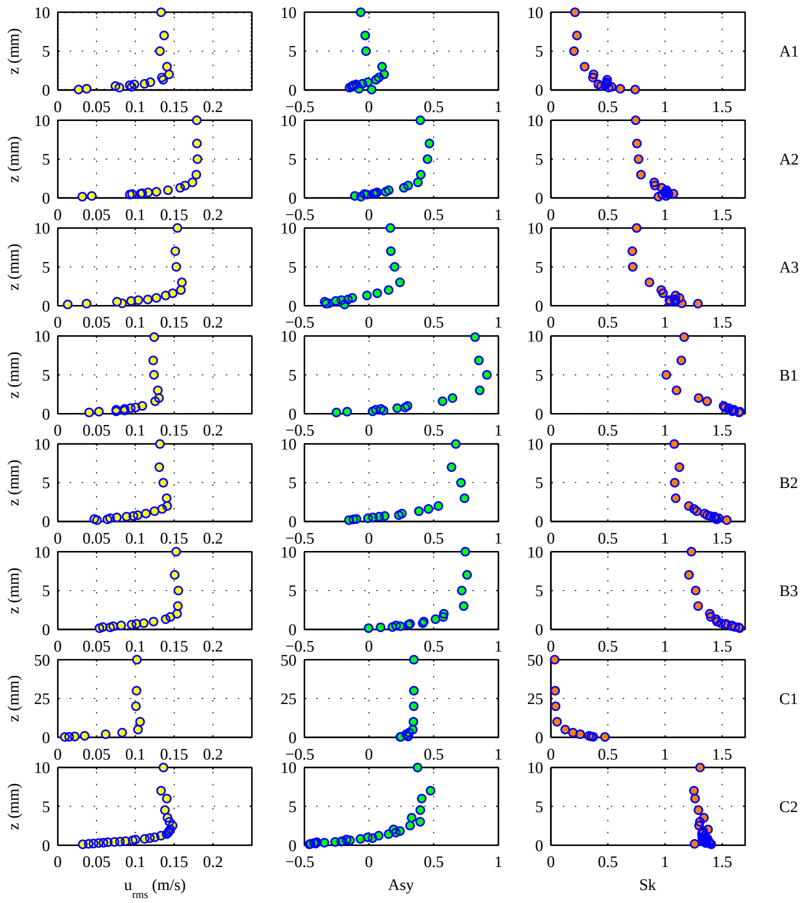

Figure 7. Vertical profiles of u_{rms} velocity (left), Asymmetry (middle) and Skewness (right), conditions indicated on the right. Note the different vertical scale for condition C1.

Figure 7 shows vertical profiles of the u_{rms}, skewness and asymmetry for all of the test conditions. It is evident from nearly all conditions that *Asy* and *Sk* are largely constant above the level of maximum u_{rms} velocity (~ boundary layer thickness) while below this level both quantities change rapidly with elevation above the bed. In all cases the near-bed reduction in asymmetry is accompanied by an increase in near-bed skewness, in agreement with the findings of Henderson et al. (2004) and Berni et al. (2013). Free-stream values of *Sk* and *Asy* differ per condition since for a given water depth both factors depend strongly on the wave height and period (Ruessink et al., 2012). The results seem to support the presence of an additional effect of spectral width as conditions A2, B2 and C2 show different *Sk* and *Asy* in the free-stream and profile development, despite having the same (significant) wave height and peak (or mean) wave period.

Low frequency contributions to the overall velocity skewness and asymmetry in the boundary layer are very small. For example, Figure 8 shows the *Sk*, *Asy* and u_{rms} profiles for the low and high frequency components of condition B3, including the (overall) phase-averaged velocity as shown in Figure 7. Differences between the phase-averaged velocity and its high frequency component are small, especially close to the bottom (z < 2mm). As shown in Rocha et al. (2013), the relative contribution of the low frequency components to *Sk* and *Asy* increases closer to the shoreline, where the low-frequency wave height becomes relatively larger compared to the high-frequency short waves.

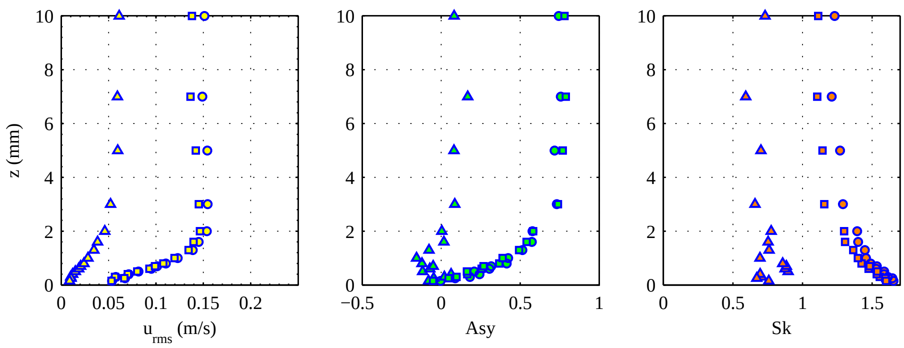

Figure 8. Vertical profiles of u_{rms}, skewness and asymmetry for condition B3. Circles: phase-averaged velocity; squares: high frequency (short wave) contribution; triangles: low frequency contribution

Henderson et al. (2004) showed, when decomposing the velocity time-series into its Fourier components, that the conversion from free-stream asymmetry to near-bed skewness occurs as a result of a frequency-independent phase shift of the Fourier components. The phase shift leads to a frequency-dependant time-shift of the components, which consequently changes the shape of the velocity time-series. The assumption of frequency independency was based on comparing free-stream velocities with the near bed velocities generated by a 1DV turbulence model, which showed that the phase lead and attenuation remained fairly constant over the energetic part of the spectrum they considered. Based on the assumption Henderson et al. derived a linear relationship between the near-bed skewness and free-stream asymmetry, which in non-dimensional form is as follows (Berni et al., 2013)

$$\frac{Sk(z_b)}{Sk_\infty} = \cos\phi(z_b) + \sin\phi(z_b)\frac{Asy_\infty}{Sk_\infty} \tag{5}$$

with z_b an elevation close to the bed and ϕ the near-bed velocity phase-lead over the free-stream velocity. Eq. (5) is based on the assumption that both the ϕ and the velocity attenuation, i.e. $K(z_b) = u_{rms}(z_b)/u_{rms,\infty}$, are frequency-independent. Berni et al. (2013) showed Eq. (5) to be valid for their measured boundary layer velocities over mobile beds, and showed it also to hold, albeit less accurately, at higher elevations above the bed. Using the laminar Stokes solution Berni et al. also deduced a linear relationship between near-bed skewness and asymmetry, except the linear relation could not be represented through Eq. (5) since, at their near bed location ($z << \delta$), both the offset and the slope were equal to 1, i.e.

$$\frac{Sk(z_b)}{Sk_\infty} = a + b\frac{Asy_\infty}{Sk_\infty} \tag{6}$$

with $a = b = 1$. At higher elevations above the bed the assumption of frequency-independency does not hold for laminar flow, as follows directly from the Stokes solution for each harmonic component (see e.g. Nielsen, 1992; Svendsen, 2006)

$$K_n(z) = 1 - e^{-z/\delta_n}\cos\left(z/\delta_n\right) \tag{7}$$

$$\phi_n(z) = \tan^{-1}\left[\frac{e^{-z/\delta_n}\sin(z/\delta_n)}{1 - e^{-z/\delta_n}\cos(z/\delta_n)}\right] \tag{8}$$

thus, both attenuation and phase-lead depend on the frequency through $\delta_n = (n2\nu/\omega)^{0.5}$. Note that $K_n(z) = 1 - Re(D_n(z))$ with $D_n(z)$ the laminar version of the complex velocity defect in Eq. (1) applied to the n'th harmonic, similarly the numerator on the right hand side of Eq. (8) is equal to the imaginary part of $D_n(z)$. Eq. (7) means that all K_n fall on one line when plotted as a function of the non-dimensional height z/δ_n (which is also the case for ϕ_n is plotted versus z/δ_n), or in other words K_n is frequency-independent as a function of z/δ_n. If there is an analogy between the attenuation of the individual harmonics K_n and the attenuation K based on u_{rms} as per Berni et al., then a linear relationship such as Eq. (4) also holds at higher elevations, but with skewness as a function of the non-dimensional height above the bed, z/δ. The latter relationship can be verified at different non-dimensional elevations above the bed using the data presented in Figure 7. However, it is not obvious for the bichromatic and especially the random wave conditions which wave period the length scale δ should be based on, and whether it should include a roughness contribution according to Eq. (2). Since K(z) can be easily obtained from the u_{rms} profiles (Fig. 6, left), one way around this issue is to select a certain value for K and for each condition take Sk at the elevation where $K(z)$ is (approximately) equal to that value. This is done in Figure 9, which shows the skewness for 4 different K values within the boundary layer (thus corresponding to 4 different z/δ elevations) and for reference the free-stream elevation which corresponds to $K = 1$, and the linear relationship found by Berni et al. which corresponds to $K \approx 0$ (and $a = 1$ and $b = 1$ in Eq. (6)). The elevation corresponding to $K \approx 1$ represents the elevation (as seen from the bed upwards) at which u_{rms} is equal to its free-stream value, thus representing an elevation still within the boundary layer. The level corresponding to $K = 1$ is the free-stream level which, by definition, leads to $Sk_K/Sk_\infty = 1$.

It needs mentioning that that the straight lines in Figure 8 are simply obtained from a linear fit to the data, thus the fit is of course dominated by the large values (condition C1). Nevertheless, the other conditions do seem to support a linear relationship between the skewness and asymmetry ratios. Part of the scatter for those conditions can be attributed to the relatively coarse vertical resolution of the measurements near the bed where the velocity gradient is high, so the elevations at which Sk was obtained do not correspond exactly to the listed K values (which represent the average K value for all conditions). Furthermore, note that condition A1 is omitted in Figure 9 since it had negative Asy_∞, and that generally the largest outliers are caused by the two remaining random wave conditions (A2 and A3) which are highlighted by the cross symbols.

When setting the slope a of the best fit lines equal to tanϕ we (tentatively) obtain values of ϕ = 15°, 25°, 33° and 41° corresponding to $K \approx 1$, 0.8, 0.6 and 0.4, and for the offset we obtain b = 0.91, 0.97, 1.0 and 1.0 respectively. This correlation between K (or z/δ) and values obtained for ϕ indicate there could be a relation between ϕ and Eq. (6), at least for the bichromatic and regular wave conditions, and restricted of course to the transitional flow conditions considered here. When the corresponding LDV measurements are processed, Figure 8 will be supplemented with more data together with a more appropriate (unbiased) fitting technique in order to confirm these values for a and b. A simple relationship between the skewness in the boundary layer and skewness and asymmetry in the free-stream could be very useful for the development of sediment transport, especially when valid for rough turbulent flow conditions.

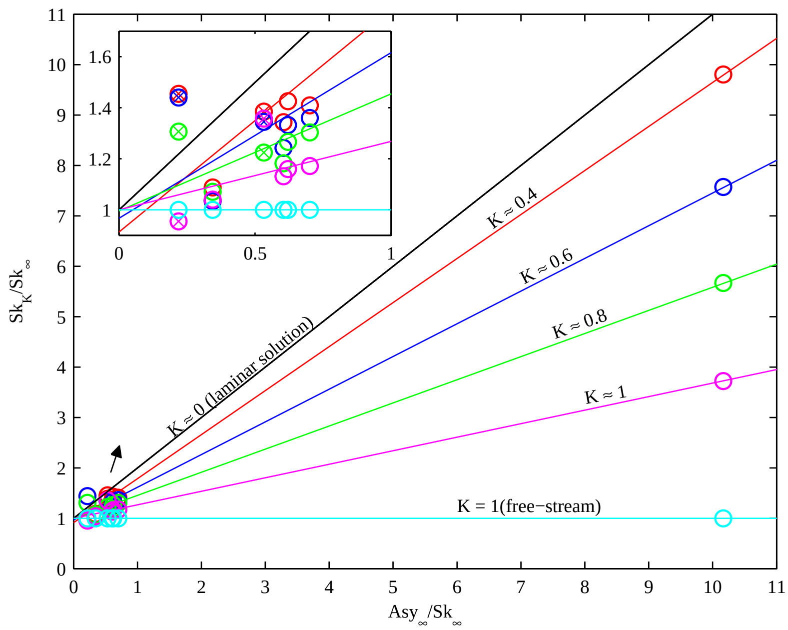

Figure 9. Boundary layer to free-stream skewness ratio as a function of free-stream asymmetry to skewness ratio. Here the Sk_K is the skewness taken at an elevation where the attenuation K (= $u_{rms}/u_{rms\infty}$) is closest to the value indicated along the straight lines, which represent the best linear fit. The black line represents the near-bed ($z << \delta$) values from the laminar solution of Berni et al. (2013).

4. Conclusion

Wave boundary layer velocities have been measured in a 110m long wave flume for a series of random, bichromatic and regular wave conditions on a 1:80 sloping concrete beach. Measurements were made with a 2-component Laser Doppler Anemometry system at a fixed location along the beach, located within the surfzone for most wave conditions. Velocity time-series show general features of oscillatory boundary layer flow such as the near bed overshoot and phase-lead. Low-frequency infragravity motions generate relatively large velocities above the bed (~10mm), but due to their relatively large boundary layer thickness the velocities closer to the bed are dominated by the high-frequency short waves. Onshore boundary layer streaming is observed and is accompanied by an offshore-directed return flow at higher elevations for most conditions. For some conditions non-zero time-averaged vertical velocities indicate there were secondary flow patterns as a result of cross-modes in the wave flume. Vertical profiles of velocity skewness and asymmetry remain constant in the free-stream but rapidly change within the boundary layer. For all conditions the velocity asymmetry decreases within the boundary layer and is coincided with an increases in velocity skewness. In agreement with a recent study by Berni et al. (2013) a linear relationship seems to exist between the near-bed velocity skewness and the velocity asymmetry and skewness in the free-stream. When the vertical coordinate is made non-dimensional by the viscous length scale, the data indicates that the linear relationship might hold at higher elevations above the bed. Corresponding LDV measurements made at another location along the fixed beach will be used to confirm the relationship.

Acknowledgements

Thanks to all Deltares technicians and staff members for their support during the GLOBEX experiment. Robert Jaryczewski of Dantec Dynamics UK is gratefully acknowledged for his help with setting-up the new LDA system on site for its inaugural experiment. This work is supported by the European Community's Seventh Framework Programme through the grant to the budget of the Integrated Infrastructure Initiative Hydralab IV, Contract no. 261520.

References

Abreu, T., Silva, P.A., Sancho, F., Michallet, H., Vasconcelos, L., 2012. Modelling horizontal velocities within the wave bottom boundary layer. Proceedings of the 23rd IASTED International Conference on Modelling and Simulation, ACTA Press, Banff, Canada.

Berni, C., E. Barthélemy, Michallet, H., 2013. Surf zone cross-shore boundary layer velocity asymmetry and skewness: an experimental study on a mobile bed, *Journal of Geophysical Research*, 118, doi:10.1002/jgrc.20125.

Dixen, M., Hatipoglu, F., Sumer, B.M., Fredsøe, J., 2008. Wave boundary layer over a stone-covered bed. *Coastal Engineering,* 55, 1–20.

Henderson, S.M., Allen, J.S., Newberger, P.A., 2004. Nearshore sandbar migration predicted by an eddy-diffusivity boundary layer model. *Journal of Geophysical Research,* 109(C06024).

Jensen, B. L., Sumer, B.M., Fredsøe, J., 1989. Turbulent oscillatory boundary layers at high Reynolds numbers. *Journal of Fluid Mechanics*, 206, 265–297.

Jonsson, I.G., Carlsen, N.A., 1976 Experimental and theoretical investigations in an oscillatory turbulent boundary layer. *Journal of Hydraulic Research,* 14, 45–60.

Klopman, G., 1994. Vertical structure of the flow due to waves and currents. Progress report, H 840.30, Part 2, Delft Hydraulics, The Netherlands.

Kranenburg, W.M., Ribberink, J.S., Schretlen, J.J.L.M., Uittenboogaard, R.E., 2013. Sand transport beneath waves: The role of progressive wave streaming and other free surface effects. *Journal of Geophysical Research*, 118, 1-18, doi:10.1029/2012JF002427.

Longuet-Higgins, M.S., 1953. Mass transport in water waves. *Philos. Trans. R. Soc. London Ser. A.,* 245, 531-581.

Malarkey, J., Davies, A.G., 2012. Free-stream velocity descriptions under waves with skewness and asymmetry. *Coastal Engineering*, 68, 78-95.

Nielsen, P., 1992. Coastal bottom boundary layers and sediment transport. Advanced Series on Ocean Engineering, vol. 4. World Scientific.

Nielsen, P., Guard, P., 2010. Vertical scales and shear stresses in wave boundary layers over movable beds. *Proceedings 32nd International Conference on Coastal Engineering,* Shanghai.

O'Donoghue, T., Wright, S., 2004. Flow tunnel measurements of velocities and sand flux in oscillatory sheet flow for well-sorted and graded sands. *Coastal Engineering*, 51, 1163-1184.

Ribberink, J.S., Al-Salem, Al-Salem, A.A., 1994. Sediment transport in oscillatory boundary layers in cases of rippled beds and sheet flow. *Journal of Geophysical Research*, 99(C6), 12,707-12,727.

Rocha, M., Michallet, H, Silva, P.A., Abreu, T., Barthélemy, E., 2013. Nonlinearities of short and long waves across the shoaling, surf and swash zones: large-scale physical model results. *Proceedings Coastal Dynamics 2013.*

Ruessink, B.G., Michallet, H., Abreu, T., Sancho, F., van der A, D.A., van der Werf, J.J., Silva, P.A., 2011. Observations of velocities, sand concentrations, and fluxes under velocity-asymmetric oscillatory flows. *Journal of Geophysical Research*, 116, C03004, doi:10.1029/2010JC006443.

Ruessink, B.G., Ramaekers, G., van Rijn, L.C., 2012. On the parameterization of the free-stream non-linear wave orbital motion in nearshore morphodynamic models. *Coastal Engineering*, 65, 56-63.

Ruessink, B.G., Michallet, H., Bonneton, P., Mouazé, D., Lara, J., Silva, P.A., Wellens, P., 2013. GLOBEX: Wave dynamics on a gently sloping laboratory beach. *Proceedings Coastal Dynamics 2013.*

Sleath, J.F.A., 1970. Velocity measurements close to the bed in a wave tank. *Journal of Fluid Mechanics*, 42, 111–123.

Sleath, J.F.A., 1987. Turbulent oscillatory flow over rough beds. *Journal of Fluid Mechanics*, 182, 369–409.

Svendsen, I.A., 2006. Introduction to neashore hydrodynamics. Advanced Series on Ocean Engineering, vol. 24. World Scientific.

Van der A, D.A., O'Donoghue, T., Ribberink, J.S., 2010. Measurements of sheet flow transport in acceleration-skewed oscillatory flow and comparison with practical formulations, *Coastal Engineering*, 57, 331-342.

Van der A, D.A., O'Donoghue, T., Davies, A.G., Ribberink, J.S., 2011. Experimental study of the turbulent boundary layer in acceleration-skewed oscillatory flow. *Journal of Fluid Mechanics*, 684, 251-283.

Van Thiel de Vries, J.S.M., van Gent, M.R.A., Walstra, D.J.R., Reniers, A.J.H.M., 2008. Analysis of dune erosion processes in large-scale flume experiments. *Coastal Engineering,* 55, 1028-1040.

Yu, X., Hsu, T.-J., Hanes, D.M., 2010. Sediment transport under wave groups: Relative importance between nonlinear waveshape and nonlinear boundary layer streaming. *Journal of Geophysical Research,* 115(C02013).